PERGAMON

Chemical Engineering Science 55 (2000) 223–231

Chemical Engineering Science

Spatio-temporal patterns in a reaction–diffusion system with wave instability

Milos Dolnik[a,b,*], Anatol M. Zhabotinsky[a], Arkady B. Rovinsky[a], Irving R. Epstein[a]

[a]*Department of Chemistry and Volen Center for Complex Systems, Brandeis University, Waltham, MA 02454-9110, USA*
[b]*Department of Biomedical Engineering and Center for BioDynamics, Boston University, 44 Cummington St., Boston, MA 02215, USA*

Received 29 March 1999; accepted 1 April 1999

Abstract

We utilize a simple three-variable reaction–diffusion model to study patterns that emerge beyond the onset of the (short-)wave instability. We have found various wave patterns including standing waves, traveling waves, asymmetric standing–traveling waves and target patterns. We employ both periodic and zero flux boundary conditions in the simulations, and we analyze the patterns using space–time two-dimensional Fourier spectra. A fascinating pattern of waves which periodically change their direction of propagation along a ring is found for very short systems. A related pattern of modulated standing waves is found for systems with zero flux boundary conditions. In a two-dimensional system with small overcriticality we observe a wide variety of standing wave patterns. These include plain and modulated stripes, squares and rhombi. We also find standing waves consisting of periodic time sequences of stripes, rhombi and hexagons. The short-wave instability can lead to a much greater variety of spatio-temporal patterns than the aperiodic Turing and the long-wave oscillatory instabilities. For example, a single oscillatory cycle may display all the basic patterns related to the aperiodic Turing instability — stripes, hexagons and inverted hexagons (honeycomb) — as well as rhombi and modulated stripes. A rich plethora of patterns is seen in a system with cylindrical geometry — examples include rotating patterns of standing waves and counter-propagating waves.

1. Introduction

Pattern formation in reaction–diffusion systems (RDS) has been the subject of intense study for the past several decades (Nicolis & Prigogine, 1977; Haken, 1978; Kuramoto, 1984; Ross, Müller & Vidal, 1988; Swinney & Krinsky, 1991; Kapral & Showalter, 1995). In RDS, three types of instabilities of a spatially uniform steady state are responsible for a variety of patterns which can be classified as follows: (i) oscillatory in time and uniform in space, connected with the space-independent Hopf bifurcation (ii) stationary in time and periodic in space, associated with the aperiodic Turing bifurcation and (iii) oscillatory in space and time. All these instabilities were studied by Turing in his seminal paper (Turing, 1952). Of the three, the oscillatory instability at finite wave number, i.e., the short-wave instability has been the least studied.

The short-wave instability has been found in binary fluid convection and in electroconvection in liquid crystals (Cross & Hohenberg, 1993). Recently, standing waves and other spatio-temporal patterns connected with this type of instability have been found in heterogeneous oscillatory reactions when diffusion of the autocatalyst is supplemented by a global negative feedback. Standing waves in the concentration of carbon monoxide have been found during oxidation on the surface of a Pt monocrystal (Jakubith, Rotermund, Engel, von Oertzen & Ertl, 1990). These standing waves were also predicted by a mathematical model that takes into account the surface reactions, surface diffusion of the autocatalyst and global coupling through the gas phase (Levin & Zou, 1993; Falcke, Engel & Neufeld, 1995). Standing waves were observed during electrochemical dissolution of nickel (Lev, Sheintuch, Pismen & Yarnitzky, 1988), and various relevant patterns were found during the atmospheric oxidation of hydrogen, propylene, methylamine and ammonia on heated metallic wires

* Corresponding author. Department of Chemistry & Volen Center for Complex Systems, Brandeis University, Waltham, MA 02454-9110, USA. Tel.: 001-781-736-2546; fax: 001-781-736-2516.
E-mail address: dolnik@brandeis.edu (M. Dolnik)

0009-2509/00/$ - see front matter
PII: S0009-2509(99)00318-8

and ribbons (Cordonier, Schuth & Schmidt, 1989; Cordonier & Schmidt, 1989; Philippou, Schultz & Luss, 1991; Graham, Lane & Luss, 1993).

Luss and coworkers performed systematic simulations with simple models of relaxation oscillators supplemented with diffusion and global negative feedback. They found various types of standing waves, target patterns and some more complicated patterns (Middya, Graham, Luss & Sheintuch, 1993; Middya, Luss & Sheintuch, 1994; Middya & Luss, 1995).

Recently, we have developed and studied a model of a simple reaction–diffusion system that contains a relatively large domain of the wave instability (Zhabotinsky, Dolnik & Epstein, 1995; Dolnik, Zhabotinsky & Epstein, 1996a,b; Dolnik, Rovinsky, Zhabotinsky & Epstein, 1999). Here, we describe and review our work on patterns obtained from one- and two-dimensional simulations of this model. Depending on the geometry of the system and on the overcriticality, the model can generate traveling and standing waves, modulated waves, alternating waves on rings, asymmetric standing-traveling wave patterns and target patterns. To find general conditions for generation of target patterns near the onset of the wave instability, we analyze the corresponding amplitude equations.

2. Model

The model that exhibits the short wave instability is based on the following reaction scheme (Zhabotinsky et al., 1995):

$$X + 2Y \rightarrow 3Y, \tag{R1}$$

$$S_1 + 2Z \rightarrow X + 2Z, \tag{R2}$$

$$Y \rightarrow P_1, \tag{R3}$$

$$S_2 + X \rightarrow X + Z, \tag{R4}$$

$$Z \rightarrow P_2, \tag{R5}$$

$$X + C \rightleftarrows XC \rightarrow C + P_3, \tag{R6}$$

$$S_3 \rightarrow Y. \tag{R7}$$

Here S_i are the initial reagents; P_j are the final products; X, Y and Z are the intermediates, whose concentrations are the dynamic variables. C is a catalyst, and XC is the catalytic complex, whose reactions (R6) are assumed to be governed by Michaelis–Menten kinetics. The autocatalytic reaction (R1) is a principal source of instability in a variety of reaction schemes (Gray & Scott, 1990). The wave instability results from the additional feedback loop: Z is the catalyst for X formation (R2), while X is the catalyst for Z formation (R4). The simpler scheme (R1)–(R5) generates the wave instability in the corresponding reaction–diffusion system; however, a much larger domain of the wave instability can be obtained with the additional reactions (R6) and (R7).

The reaction–diffusion model in its dimensionless form corresponding to reaction scheme (R1)–(R7) is (Zhabotinsky et al., 1995):

$$\frac{\partial x}{\partial t} = m\left(-xy^2 + z^2 - \frac{ax}{g+x}\right) + d_x \Delta x,$$

$$\frac{\partial y}{\partial t} = n(xy^2 - y + b) + d_y \Delta y$$

$$\frac{\partial z}{\partial t} = x - z + \Delta z, \tag{1}$$

where Δ is the Laplacian operator.

In the simulations presented here we set $d_x = d_y = 0$, which gives the largest domain of the wave instability. We keep constant the following parameters: $g = 1 \times 10^{-4}$, $a = 0.9$, $b = 0.2$, $n = 15.5$, and we vary the parameter m and size of the system. The value $m_c \approx 28.56915$ corresponds to the short-wave bifurcation and $m_h \approx 26.79767$ to the spatially independent Hopf bifurcation. The domain of pure short-wave instability is found for $m_h < m < m_c$. We refer to $\varepsilon = (m_c - m)/m_c$ as the overcriticality. The maximum of the dispersion curve (see Fig. 1), occurs at a wavelength of approximately 3.426 space units. We refer to this value as the basic wavelength in what follows. The basic wavelength is nearly independent of m in the domain of pure short-wave instability. The period of oscillation is about 0.6 time units; this value does not change significantly in our range of overcriticality.

We perform a global qualitative study of pattern formation in a parameter domain beyond the onset of the wave instability both in one- and two-dimensional systems. Our goal is to find stable patterns with relatively large basins of attraction.

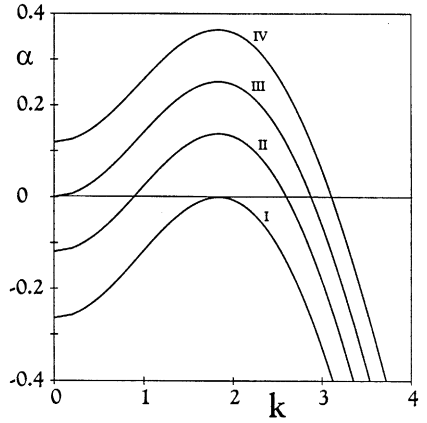

Fig. 1. Dispersion curves for real parts of complex eigenvalues. I – wave bifurcation, overcriticality $\varepsilon = 0$; II – pure wave instability, $\varepsilon = 0.034$; III – homogeneous Hopf bifurcation, $\varepsilon = 0.062$, IV – wave instability coexists with spatially uniform oscillatory instability, $\varepsilon = 0.09$.

3. Waves in one-dimensional systems

3.1. Zero flux boundary conditions

We utilize a homogeneous steady state as the initial condition in a one-dimensional system with zero flux boundary conditions. The steady state value of x is perturbed with amplitude 0.2 at a single gridpoint on one wall. The simulations are run for 500 time units at each point.

Fig. 2 presents a structure diagram in the overcriticality — length parametric plane. The standing waves (SW), shown in Fig. 3a, are stable at low overcriticality. For instance, at $\varepsilon = 0.01$, not only asymmetric local perturbations but also symmetric perturbations result in SW with wavelength $\lambda = L/6$.

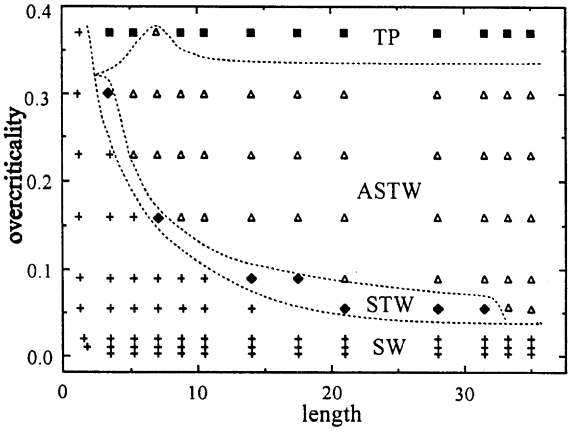

Fig. 2. Patterns in one-dimensional system with zero flux boundary conditions. Symbols: + – standing waves, SW; ◆ – standing–traveling waves, STW; △ – aperiodic standing–traveling waves, ASTW; ■ – target patterns, TP. Dashed lines are estimated boundaries of domains with different patterns.

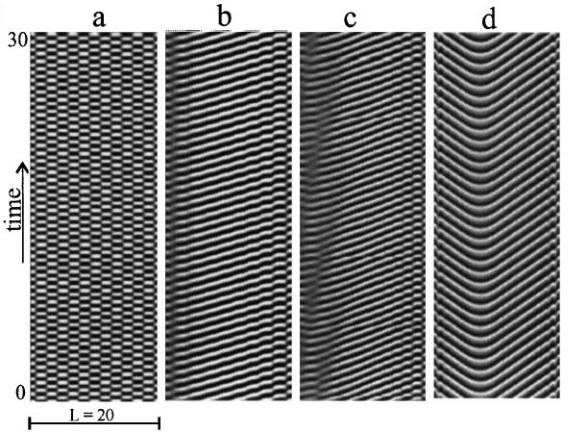

Fig. 3. Stationary spatio-temporal patterns in one-dimensional system with zero flux boundary conditions, system length $L = 20$. Values of x are quantified with gray levels: white corresponds to the maximum value of x, black to the minimum value. (a) Standing waves, $\varepsilon = 0.01$; (b) standing–traveling waves, $\varepsilon = 0.09$; (c) aperiodic standing–traveling waves, $\varepsilon = 0.23$; (d) target patterns, $\varepsilon = 0.37$.

With increasing system length (L) or overcriticality ε (decrease of m), the basin of attraction of SW shrinks, and asymmetric patterns appear. These patterns are intermediate between SW and target patterns (TP). Most of the pattern displays a strong dominance of one of the constituent traveling waves, which forms a TP. We term these patterns standing–traveling waves (STW), and Fig. 3b shows an example of STW.

A further increase of the overcriticality, $0.09 \leqslant \varepsilon \leqslant 0.30$, causes STW to become aperiodic in time. Fig. 3c shows an example of aperiodic STW (ASTW). For overcriticality above $\varepsilon = 0.30$ the stable patterns are target patterns for length $L = 8$ and larger. Target patterns consist of three regions (see Fig. 3d): a leading center (source), a domain occupied by traveling waves and a region adjacent to the point of collision of the waves with walls (sink). The sink region displays a strongly decaying standing wave (Zhabotinsky et al., 1995). The sizes of the source and sink regions are practically independent of the system length.

3.1.1. Modulated standing waves

In a short system with zero flux boundary conditions the standing waves occupy the largest part of the ε, L-diagram (see Fig. 2). We have found two domains of modulated standing waves (MSW) when the system length is between 0.5 and 1.5 times the characteristic wavelength. The domains of MSW are too small to be seen clearly in Fig. 2 (Dolnik et al., 1996a). One domain of MSW separates domains of the half-wavelength SW and the one wavelength SW; another domain is situated inside the region of STW.

Fig. 4a shows an example of MSW. One can see the modulation period determined by alternating short-lived nodes. The modulation cycle consists of four parts: During the first part, the wavefront propagates to the right; in the second part, a short-lived asymmetric standing wave appears with a node in the right half of the system; during the third phase of the cycle, the wavefront propagates to the left; and in the fourth part of the cycle, the asymmetric standing wave has its node in the left half of the system.

We employ fast Fourier transformation (FFT) to analyze patterns of MSW. We choose the number of sampled points to be 2048 for the time dimension (with a sampling step of 0.05 time units), and 128 for the space dimension. Fig. 4b displays the Fourier spectrum of the MSW. Major peaks are found at (k_1, f_1), $(0, f_1 - f_m)$ and $(2k_1, f_1 + f_m)$, where the basic wave number is $k_1 = 2\pi \cdot 0.2273$, the frequency of oscillations is $f_1 = 1.289$, and the frequency of modulation is $f_m = 0.137$.

3.1.2. Target patterns

To better understand the more general properties of the wave instability, especially as a mechanism of generating target patterns, we undertook a study of the

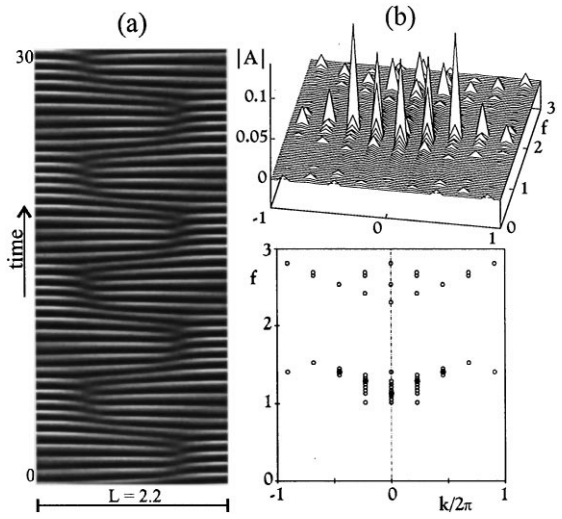

Fig. 4. Modulated standing waves in a one-dimensional system with zero flux boundary conditions, $\varepsilon = 0.30$. (a) Space-time plot, (b) Fourier spectrum of the MSW; bottom part displays locations of major Fourier spectrum components. Symbols indicate amplitude of major components: ○ $0.01 \leqslant |A| < 0.03$, ● $0.03 \leqslant |A|$.

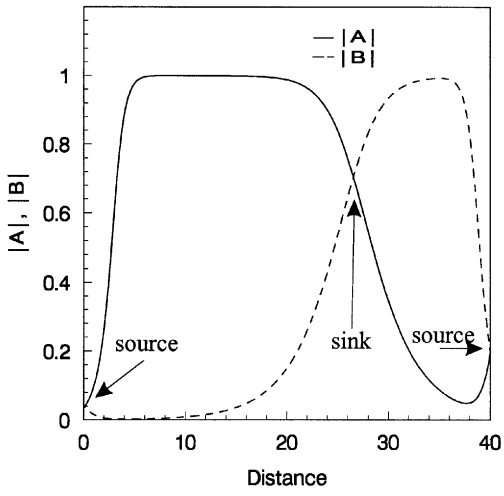

Fig. 5. Amplitude profiles in complex Ginzburg–Landau equations for small overcriticality: $\delta/\delta_{\text{crit}} = 0.25$. Stationary sources of target patterns are attached to zero-flux boundaries.

corresponding Ginzburg–Landau equations (GLE). The standard form of GLE (Cross & Hohenberg, 1993) becomes after rescaling (Rovinsky, Zhabotinsky & Epstein, 1997):

$$A_t = A - (1 + \mathrm{i}\alpha)|A|^2 A - \gamma(1 + \mathrm{i}\beta)|B|^2 A - A_x + \delta(1 + \mathrm{i}\eta)A_{xx},$$

$$B_t = B - (1 + \mathrm{i}\alpha)|B|^2 B - \gamma(1 + \mathrm{i}\beta)|A|^2 B + B_x + \delta(1 + \mathrm{i}\eta)B_{xx}. \quad (2)$$

This pair of coupled GLE describes the dynamics of a generic system close to the wave bifurcation, not just of the system described by model (1). Here, the overcriticality is denoted as δ. The variables A and B are the amplitudes of the emerging waves: A is the complex amplitude of the mode traveling to the right, and B is that of the mode traveling to the left. The zero-flux boundary conditions of the original reaction-diffusion system are translated in the case of the GLE into the following form (Rovinsky et al., 1997):

$$[A_x]_{x=0,L} = -[B_x]_{x=0,L}$$

$$[A]_{x=0,L} = [B]_{x=0,L}. \quad (3)$$

It is known that an infinite system described by Eq. (2) can only support stable target patterns for large overcriticality $\delta > \delta_{\text{crit}}$, i.e., when the validity of the GLE description of a reaction–diffusion system is questionable. Our main finding is that, in a finite system, zero-flux boundary conditions can make target patterns stable even at small overcriticality. An example of such stable patterns attached to zero-flux boundaries is shown in Fig. 5. While it was previously thought that target patterns are nucleated on inhomogeneities that locally change the kinetic parameters of the system, our results show that "neutral" walls may also be pacemakers in the case of the wave instability.

Stable sources of waves are found at relatively small values of the parameter γ, which characterizes the mode coupling. At larger values of γ the source attached to the boundary becomes oscillating, as illustrated in Fig. 6a. At sufficiently small overcriticality and still larger γ the pattern takes the form of alternating wave packets (Fig. 6b). Fig. 6c shows the domains of different patterns in a finite system with zero-flux boundary conditions.

3.2. Periodic boundary conditions

Traveling waves (TW) and TP are stable solutions in the one-dimensional system (Eq. (1)) with periodic boundary conditions. When the system length or overcriticality changes, traveling waves are forced to adjust to this change. This adjustment can result in a change in the wavelength and/or in the number of wave periods on the ring, or in development of modulation.

3.2.1. Modulated and alternating waves on a ring

Fig. 7a shows a modulated traveling wave, which develops from the initial conditions corresponding to the unmodulated two wavelength traveling wave. The transient period is relatively long, with more than 50 time units of the almost unchanged simple traveling wave pattern, after which the modulation becomes visible. Only after more than 200 time units is the stationary pattern of modulated TW (MTW) with noticeable slow waves of modulation established. Fig. 7b presents an overlay of 20 consecutive y-profiles taken at intervals of 0.025 time

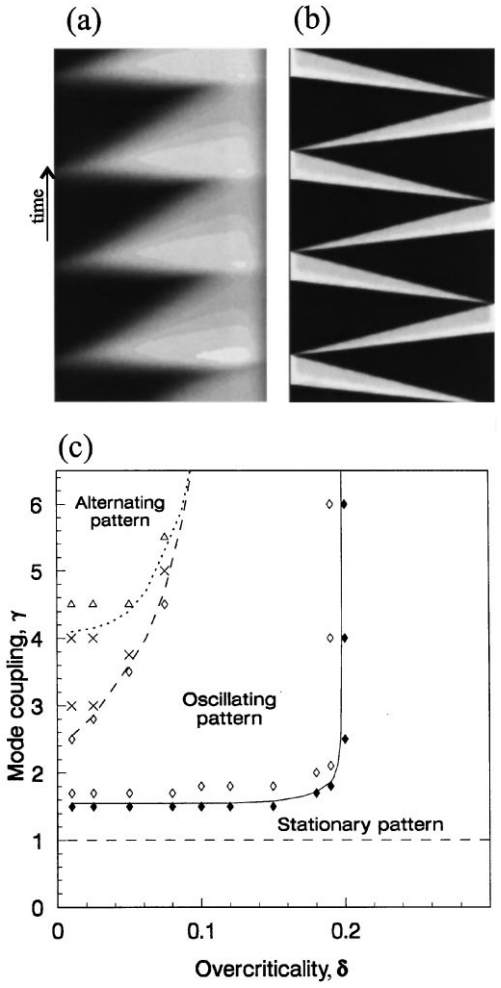

Fig. 6. Solutions of complex Ginzburg–Landau equations. (a) An oscillating source in a system with zero-flux boundary conditions. The gray levels represent the value of $|A|$, i.e. the amplitude of the wave traveling to the right, with the dark corresponding to a low value, and the light to a high value. Parameters: $\delta/\delta_{\mathrm{crit}} = 0.5, \gamma = 2$. (b) Alternating wave packets. The gray levels represent the value $|A| + |B|$, i.e. the sum of amplitudes of waves traveling to the right and to the left. In these calculations, when one of the amplitudes was high the other was near zero. Parameters: $\delta/\delta_{\mathrm{crit}} = 0.025, \gamma = 10$. (c) The domains of stationary, oscillating and alternating sources. The area between the dashed and dotted lines is a domain of complex alternating sources.

units. Both the spatio-temporal pattern (Fig. 7a) and the overlay of profiles (Fig. 7b) show a strong modulation of the speed and the amplitude of the traveling wave. Fig. 7c shows the Fourier spectrum of the MTW, with the largest peak at the basic wave number $k_1 = 2\pi \cdot 0.28575 = 4\pi/L$ and frequency $f_1 = 1.0449$. The spectrum further reveals pronounced second and third harmonics of the basic wave and the sidebands. The spectrum shows that the basic traveling wave is modulated by a wave whose wave number K_1 and frequency F_1 can be determined from the sideband location (k_{1s}, f_{1s}): $K_1 = k_1 - k_{1s} = 2\pi \cdot 0.575 = 2k_1$ and $F_1 = f_1 - f_{1s} = 0.1375$. The first right sideband of the second harmonic of the basic wave is a zero mode.

The domain of MTW with system length $L \approx 4$ contains one wavelength modulated waves. For large overcriticality these modulated waves become unstable and a new pattern of alternating modulated waves (ATW) emerges. Fig. 8 shows a stationary pattern of ATW with its Fourier spectrum. The full cycle of an ATW consists of four parts: The wave travels clockwise, is transformed to a short-lived standing wave, then becomes a counter-clockwise traveling wave, and is again transformed to a short-lived standing wave. The Fourier spectrum of the ATW consists of two counter propagating basic waves, each of which is modulated by a slow wave and by a zero mode. The principal bands, which correspond to the first harmonics of the basic waves, appear at $k_1 = \pm 2\pi \cdot 0.27778$ and with maximum amplitude at $f_1 = 1.1475$.

We have not found a stationary pattern of alternating traveling waves for systems with ring size larger than $L = 5$. However, the alternating traveling waves can be seen as transients in larger rings. Fig. 9 shows a transient alternating traveling wave as it develops from the initial conditions corresponding to the unmodulated two wavelength traveling wave. The modulation becomes visible after approximately 40 time units, and for an additional 60 time units the traveling wave displays strong modulation without alternation of the direction of propagation. Then the transient alternating wave pattern emerges and lasts about 100 time units. Finally, the stationary three-wavelength traveling wave emerges (last frame of Fig. 9, top).

4. Standing waves in two-dimensional systems

We investigate a small neighborhood of the wave bifurcation with overcriticality $\varepsilon \leqslant 0.02$ in two-dimensional systems with square and rectangular geometry with zero flux boundary conditions. To reveal the stationary patterns of standing waves with the largest basins of attraction, we perform sets of 20 simulations with identical parameters and different random initial conditions. In our simulations we utilize both square and rectangular systems.

4.1. Square pattern

Fig. 10 shows a cycle of oscillation of a stable square pattern in the two-dimensional square system 20×20, at overcriticality $\varepsilon = 2.4 \times 10^{-3}$. The sequence shown consists of 12 snapshots of the x-variable; adjacent images are one twelfth of a period apart. The pattern consists of two mutually perpendicular sets of stripes that oscillate with a phase shift of $\pi/2$. The wavelength of the instantaneous pattern is close to the basic wavelength and allows exactly six wavelengths in the 20×20 system in each direction. The corresponding wave number, 1.885,

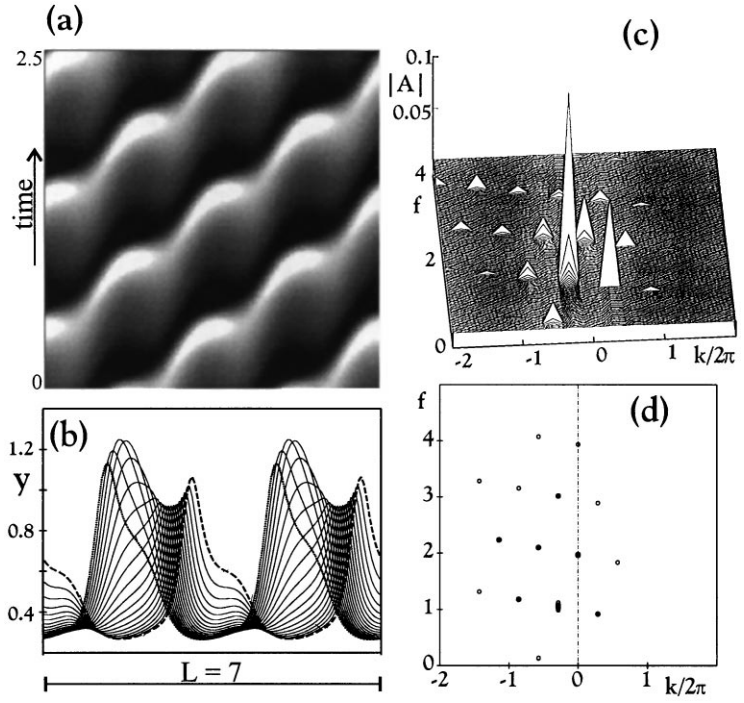

Fig. 7. Modulated traveling wave in one-dimensional system with periodic boundary conditions, $\varepsilon = 0.37$. (a) Space–time plot. (b) Overlay of 20 consecutive y-profiles taken at intervals of 0.025 time units. Dotted line – 1st profile, dashed line – 20th profile. (c) Fourier spectrum of the modulated traveling wave. (d) Locations of major Fourier spectrum components. Symbols indicate amplitude of major components: ○ $0.01 \leqslant |A| < 0.03$, ● $0.03 \leqslant |A|$. The figure shows strong modulation both of speed and amplitude of the traveling wave.

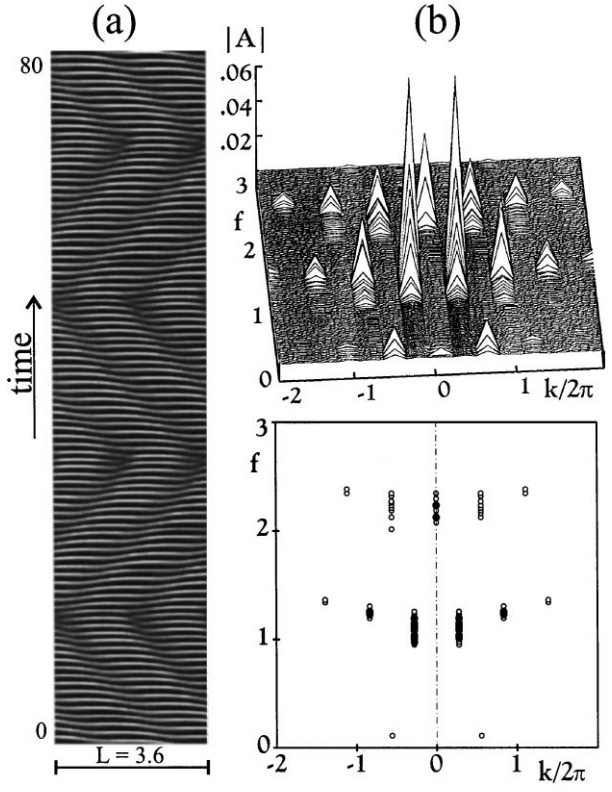

Fig. 8. Alternating traveling wave on a ring, overcriticality $\varepsilon = 0.37$. (a) Space–time plot, (b) Fourier spectrum; symbols indicate amplitude of major components: ○ $0.01 \leqslant |A| < 0.03$, ● $0.03 \leqslant |A|$.

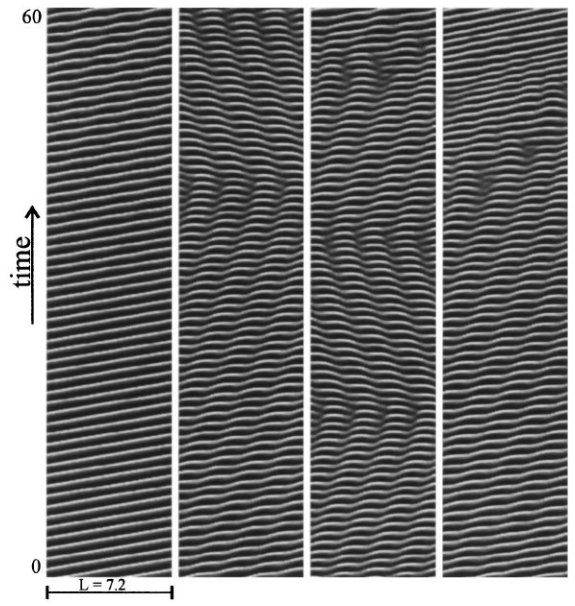

Fig. 9. Transient alternating traveling wave on a ring, $\varepsilon = 0.37$. Consecutive frames correspond to 60 time units each.

lies close to the middle of the unstable domain shown in Fig. 1. The probability for the square pattern to evolve from random initial conditions exceeds 50% in this system. With increasing overcriticality and with increasing size of the square system this probability decreases.

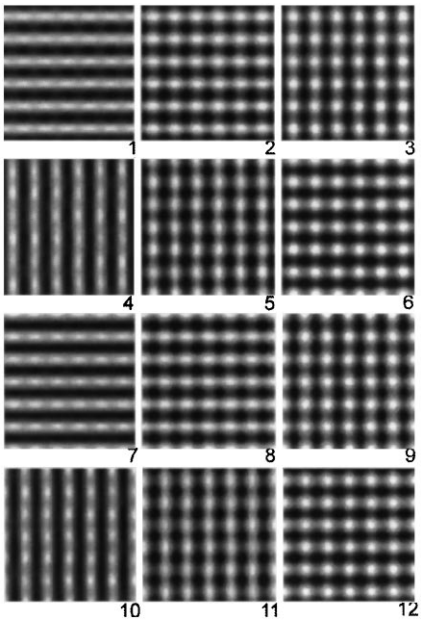

Fig. 10. Square pattern of standing waves in two-dimensional 20×20 system with zero flux boundary conditions, $\varepsilon = 2.4 \times 10^{-3}$. Adjacent images are one-twelfth period apart.

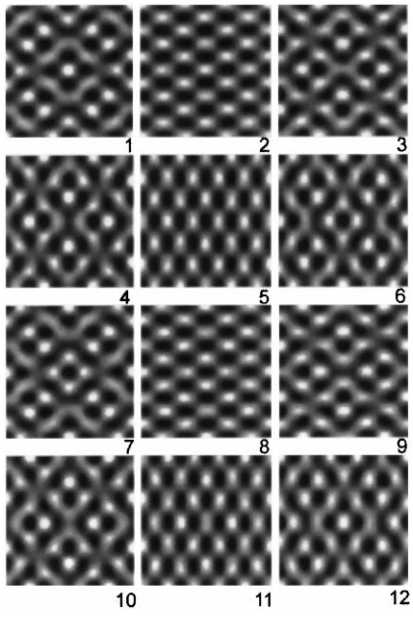

Fig. 11. Rhombic pattern of standing waves in two-dimensional 20×20 system with zero flux boundary conditions, $\varepsilon = 2.4 \times 10^{-3}$.

4.2. Rhombic pattern

Fig. 11 shows another pattern of two-dimensional SW, which evolves from random initial conditions in the square system 20×20, at overcriticality $\varepsilon = 2.4 \times 10^{-3}$. Frames 2 and 8 display a simple rhombic pattern with wavelengths $\lambda_{\text{hor}} = L/3$ in the horizontal direction and $\lambda_{\text{ver}} = L/5$ in the vertical direction; frames 5 and 11 show this pattern rotated by $\pi/2$. Other frames display complex rhombic patterns. This sequence of rhombic patterns occurred in one out of four simulations. The rhombic pattern is the most commonly found pattern for low overcriticality for the square system 40×40. This pattern often emerges from random initial conditions in rectangular systems.

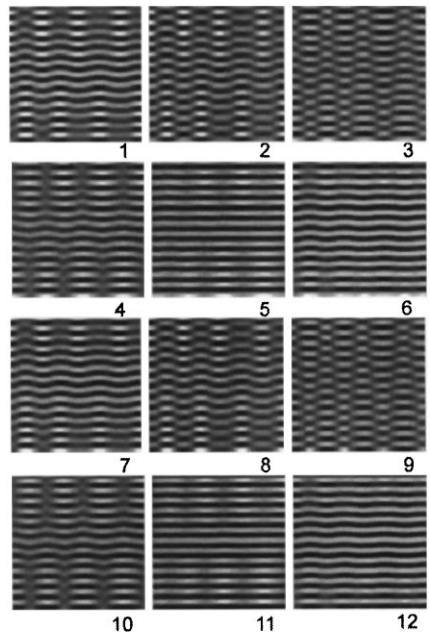

Fig. 12. Modulated stripe pattern of standing waves in two-dimensional 40×40 system with zero flux boundary conditions, $\varepsilon = 2 \times 10^{-2}$.

4.3. Modulated and unmodulated stripes

The most commonly found patterns for system 40×40 at overcriticality $\varepsilon = 2 \times 10^{-2}$ are modulated stripes, observed in more than 50% of the cases. Fig. 12 shows an example of modulated stripes for this system. The modulation is clearly visible in all frames, except in frames 5 and 11, where the instantaneous pattern is pure stripes. Although stripes are often found as transient patterns in square systems, we have seen emergence of persistent unmodulated stripes from random initial conditions only in rectangular systems. However, for uniform initial conditions with equal perturbation at every point along a side, the unmodulated stripes are always the stable pattern for both square and rectangular systems.

4.4. Hexagon-stripe patterns

Another pattern that emerges from random initial conditions only in rectangular systems is the hexagon–stripe pattern (Fig. 13). Although some of the snapshots in Fig. 13 show simple hexagonal patterns, the spatio-temporal pattern is dominated by horizontal stripes. The

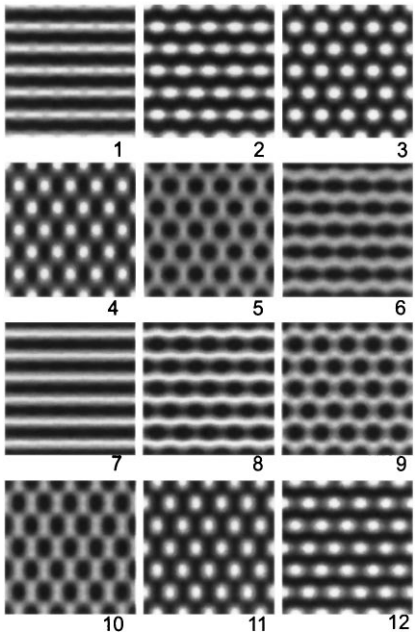

Fig. 13. Stripes–rhombi–hexagons pattern of standing waves in two-dimensional 20×19 system with zero flux boundary conditions, $\varepsilon = 2.4 \times 10^{-3}$.

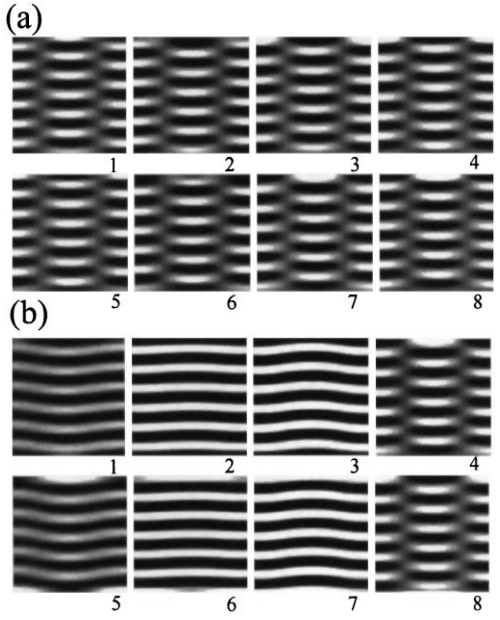

Fig. 14. Traveling waves in two-dimensional 20×20 cylindrical system. (a) Standing waves rotates around cylinder. (b) Counter-propagating waves.

oscillatory cycle of this pattern runs through simple stripes to modulated ones, then to rhombi, hexagons, rhombi, and then inverted hexagons (honeycomb), rhombi, modulated stripes and simple stripes.

5. Traveling waves on a cylinder

We further study the stable patterns formed on a cylinder (a two-dimensional system with zero flux boundary conditions along one dimension and periodic boundary conditions along the other dimension). Similarly, as for SW patterns in a two-dimensional system, we perform a large number of simulations (20) with identical parameters and different random initial conditions to reveal the patterns with the largest basins of attraction.

Fig. 14 shows the most commonly observed patterns for small overcriticality ($\varepsilon = 2.4 \times 10^{-3}$). Zero flux boundaries are on the left and right side of each frame. Fig. 14a displays a stable pattern of waves which rotates (travels) around the cylinder. The rotation can be seen in Fig. 14a as an upward shift of the pattern. The zero flux boundaries stabilize the SW pattern along the horizontal direction.

Another pattern of waves rotating around a cylinder is shown in Fig. 14b. In this case the central and side parts of the pattern are counter propagating; a pattern similar to that shown in Fig. 14a is formed at the instant when the counter-propagating waves are shifted by exactly half a wavelength (frames 4 and 8). When the counter-propagating waves are aligned, an instantaneous stripe pattern can be observed (frames 2 and 6).

6. Conclusions

The short-wave instability appears to be capable of generating a greater variety of patterns than two other, much better studied instabilities: the aperiodic Turing and the long-wave oscillatory instabilities. Our results on pattern formation in the three-variable reaction–diffusion model described above confirm this assertion. In one-dimensional systems we have found traveling and standing waves, asymmetric standing–traveling wave patterns and target patterns. With periodic boundary conditions, we observed various patterns of modulated waves and a fascinating pattern of waves that periodically change their direction of propagation along the ring.

In two-dimensional systems, we found a whole zoo of standing wave patterns immediately beyond the onset of the short-wave instability. These include plain and modulated stripes, squares and rhombi. We also find standing waves consisting of periodic time sequences of stripes and rhombi, stripes and squares, and stripes, rhombi and hexagons. In one type of these spatio-temporal patterns, a single oscillatory cycle can display all the basic patterns related to the aperiodic Turing instability — stripes, hexagons and inverted hexagons (honeycomb) — as well as rhombi and modulated stripes.

As a general rule, basins of attraction of more symmetric patterns shrink, while less symmetric patterns become stable with increasing overcriticality or system length.

Notations

a, b, g, m, n	dimensionless model parameters
A, B	amplitudes in complex Ginzburg–Landau equation
C	catalyst
d	dimensionless diffusion coefficient
f	dimensionless frequency
k	dimensionless wavenumber
L	dimensionless system length
P_j	final products
S_i	initial reagents
x, y, z	dimensionless variables
X, Y, Z	intermediates
XC	catalytic complex

Greek letters

α, β, η	coefficients in complex Ginzburg–Landau equation
γ	mode coupling
δ	overcriticality in complex Ginzburg–Landau equation
ε	overcriticality in reaction-diffusion model
λ	dimensionless wavelength

Acknowledgements

We gratefully acknowledge the support of the National Science Foundation Chemistry Division and the W. M. Keck Foundation.

References

Cordonier, G. A., Schuth, F., & Schmidt, L. D. (1989). Oscillations in methylamine decomposition on Pt, Rh, and Ir-experiments and models. *Journal of Chemical Physics*, *91*, 5374–5386.

Cordonier, G. A., & Schmidt, L. D. (1989). Thermal waves in NH_3 oxidation on a Pt wire. *Chemical Engineering Science*, *44*, 1983–1993.

Cross, M. C., & Hohenberg, P. C. (1993). Pattern formation outside of equilibrium. *Reviews in Modern Physics*, *65*, 851–1112.

Dolnik, M., Zhabotinsky, A. M., & Epstein, I. R. (1996a). Modulated standing waves in a short reaction-diffusion system. *Journal of Physical Chemistry*, *100*, 6604–6607.

Dolnik, M., Zhabotinsky, A. M., & Epstein, I. R. (1996b). Modulated and alternating waves in a reaction-diffusion model with wave instability. *Journal of Chemical Society of the Faraday Transactions*, *92*, 2919–2925.

Dolnik, M., Rovinsky, A.B., Zhabotinsky, A.M., & Epstein, I.R. (1999). Standing waves in a two-dimensional reaction-diffusion model with the short-wave instability, *Journal of Physical Chemistry*, *A*, *103*, 38–45.

Falcke, M., Engel, H., & Neufeld, M. (1995). Cluster formation, standing waves, and stripe patterns in oscillatory active media with local and global coupling. *Physics Reviews E*, *52*, 763–771.

Gray, P., & Scott, S. K. (1990). *Chemical oscillations and instabilities*. Oxford: Clarendon Press.

Graham, D., Lane, S. L., & Luss, D. (1993). Temperature pulse dynamics on a catalytic ring. *Journal of Physical Chemistry*, *97*, 7564–7571.

Haken, H. (1978). *Synergetics*. Berlin: Springer.

Jakubith, S., Rotermund, H. H., Engel, W., von Oertzen, A., & Ertl, G. (1990). Spatiotemporal concentration patterns in a surface reaction. Propagating and standing waves, rotating spirals and turbulence. *Physics Review Letters*, *65*, 3013–3016.

Kapral, R. & Showalter, K. (Eds.), (1995). Chemical waves and patterns. Dordrecht: Kluwer.

Kuramoto, Y. (1984). *Chemical oscillations, turbulence and waves*. Berlin: Springer.

Lev, O., Sheintuch, M., Pismen, L. M., & Yarnitzky, C. (1988). Standing and propagating wave oscillations in the anodic dissolution of nickel. *Nature*, *336*, 458–459.

Levine, H., & Zou, X. (1993). Catalysis at single-crystal Pt(110) surfaces: Global coupling and standing waves. *Physical Reviews E*, *48*, 50–64.

Middya, U., Graham, M. D., Luss, D., & Sheintuch, M. (1993). Pattern selection in controlled reaction-diffusion systems. *Journal of Chemical Physics*, *98*, 2823–2836.

Middya, U., Luss, D., & Sheintuch, M. (1994). Impact of global interaction and symmetry on pattern selection and bifurcation. *Journal of Chemical Physics*, *101*, 4688–4696.

Middya, U., & Luss, D. (1995). Impact of global interaction on pattern formation on a disk. *Journal of Chemical Physics*, *102*, 5029–5036.

Nicolis, G., & Prigogine, I. (1977). *Self-organization in nonequilibrium systems*. New York: Wiley.

Philippou, G., Schultz, F., & Luss, D. (1991). Spatiotemporal temperature patterns on an electrically heated catalytic ribbon. *Journal of Physical Chemistry*, *95*, 3224–3229.

Ross, J., Müller, S. C., & Vidal, C. (1988). Chemical waves. *Science*, *240*, 460–461.

Rovinsky, A. B., Zhabotinsky, A. M., & Epstein, I. R. (1997). Target patterns arising from the short-wave instability in the near-critical regimes of reaction-diffusion systems. *Physics Reviews E*, *56*, 2412–2417.

Swinney, H. L., & Krinsky, V. I., (Eds.), (1991). Waves and patterns in chemical and biological media, *Physica D*, *49* (1 & 2).

Turing, A. M. (1952). The chemical basis for morphogenesis. *Philosophical Transactions of the Royal Society B*, *237*, 37.

Zhabotinsky, A. M., Dolnik, M., & Epstein, I. R. (1995). Pattern formation arising from wave instability in a simple reaction-diffusion system. *Journal of Chemical Physics*, *103*, 10306–10314.